Accepted Manuscript

Effects of *Synechococcus* sp. cyanobacteria inert biomass on olivine dissolution: Implications for the application of enhanced weathering methods

Sebastian Weber, Raul E. Martinez

PII: S0883-2927(16)30516-9

DOI: 10.1016/j.apgeochem.2017.06.011

Reference: AG 3913

To appear in: *Applied Geochemistry*

Received Date: 23 November 2016

Revised Date: 19 June 2017

Accepted Date: 20 June 2017

Please cite this article as: Weber, S., Martinez, R.E., Effects of *Synechococcus* sp. cyanobacteria inert biomass on olivine dissolution: Implications for the application of enhanced weathering methods, *Applied Geochemistry* (2017), doi: 10.1016/j.apgeochem.2017.06.011.

Effects of *Synechococcus* sp. cyanobacteria inert biomass on olivine dissolution: implications for the application of enhanced weathering methods

Sebastian Weber and Raul E. Martinez*

Institut für Geo- und Umweltnaturwissenschaften, Mineralogie-Petrologie, Albert-Ludwigs-Universität Freiburg, D-79104 Freiburg, Germany.

*Corresponding author:
Tel.: +49 761 203 6423
E-mail address: raul.martinez@minpet.uni-freiburg.de (R. E. Martinez)

Key words: CO_2 sequestration, partially closed batch reactors, freshwater cyanobacteria, Synechococcus sp., *air bubbling, olivine dissolution, enhanced weathering*

Abstract

Chemical weathering of silicates represents an essential process of both the rock and carbon cycles. The application of this natural process on a global scale could be used to mitigate excess CO_2 in the atmosphere. This concept is known as enhanced weathering where fine mineral powder is spread over the land surface for carbonation of silicates and expected CO_2 sequestration. Within this context, organic matter, may promote or inhibit the processes of enhanced weathering, however this has not yet been fully quantified. Motivated by this knowledge gap, the present work studied the dissolution behaviour of olivine under inorganic conditions and in the presence of inert *Synechococcus* sp. biomass in batch reactor setups at various ionic strengths with a constant input of atmospheric CO_2. Olivine, which represents one of the most obvious candidates for use in enhanced weathering, showed no significant statistical differences in the release of dissolved cations for all studied organic and inorganic experimental setups. For batch reactors containing inert biomass, a moderate increase in alkalinity and pH is found with respect to the inorganic conditions, which points to the buffering of H_2CO_3 by deprotonated functional groups on the inert biomass surface. Overall, the experimental results of this study indicate a negative combined effect of inert biomass and high ionic strengths on the olivine dissolution rates in natural aquatic systems. This suggests reduced carbonation rates on the Earth's surface and a lower potential of artificially dispersed olivine powder for CO_2 sequestration.

1. Introduction

Carbon-dioxide storage via "enhanced weathering" of silicates has been proposed as a method to lower atmospheric CO_2 levels (Ferris et al. 1994; Schuiling et al. 2006; Hartmann et al., 2009; Hartmann et al., 2013). Enhanced weathering refers to the application of fine powdered silicates over the land's surface for CO_2 sequestration. The dissolution of these added minerals will produce dissolved divalent metal cations (e.g. Ca^{2+}, Mg^{2+} and Fe^{2+}) and bicarbonate to increase the alkalinity and pH of natural aqueous environments. The formation of carbonate species (e.g. HCO_3^- and CO_3^{2-}) in the presence of the dissolved divalent cations can lead to the formation of carbonate minerals, for CO_2 mineralization (Ferris et al. 1994; Golubev et al., 2005; Bachu, 2008; Bachu and Adams, 2003; Lackner, 2003; Gerdemann et al., 2007; Oelkers et al., 2008; Kelemen et al., 2011; Zhang and Bachu, 2011; Bundeleva et al., 2014; Martinez et al., 2014; Oelkers et al., 2015). Studies dealing with dissolution rates of silicates have indicated that the most efficient sources of the required divalent cations are mafic and ultramafic rocks (Ferris et al., 1994; Goff and Lacker, 1998; Awad et al., 2000; McGrail et al., 2006; Alfredsson et al., 2008; Oelkers et al., 2008; Matter et al., 2009, 2011; Schaefer et al., 2010; Gislason et al., 2010; Gysi and Stefansson, 2012; Aradóttir et al., 2012; Oskierski et al., 2013 a & b; Gislason and Oelkers, 2014). This finding has promoted a significant number of works aimed at quantifying the carbonation rates of primary silicates, such as olivine (Casey and Westrich, 1992; O'Connor et al., 2002; Park et al., 2003; Park and Fan, 2004; Jia et al., 2004; Giammar et al., 2005; Huijgen et al., 2006; Alexander et al., 2007; Dufaud et al., 2009; Garcia et al., 2010; King et al., 2010; Orlando et al., 2011; Pronost et al., 2011; Klein and Mc Collom, 2013; Martinez et al., 2014).

Olivine has been categorized as the most suitable silicate for enhanced weathering purposes given its reactivity and natural abundance (Berner et al., 1983; Pokrovsky and Schott 2000 a, b; Oelkers, 2001, 2009; Hartmann et al., 2013; Martinez et al. 2014; Eikeland et al., 2015; Oelkers et al. 2015). This silicate has shown high dissolution rates as a result of a weakly connected fabric (Berner et al., 1983; Pokrovsky and Schott 2000 a,b; Oelkers, 2001; Oelkers et al., 2009). At acidic or near neutral pH, (pH < 8), surface protonation increases >Mg-O bond lengths leading to dissolved Mg^{2+} (Liu et al., 2006; Pokrovsky and Schott 2000 a,b; Rimstidt et

al., 2012; Olsson et al., 2012; Martinez et al., 2014). Several studies investigating the mechanisms of olivine dissolution suggest that in the initial steps of olivine protonation, Mg may be released at a faster rate than SiO_4^{4-} suggesting the formation of a uniformly distributed Mg-depleted Si-rich surface layer (Wogelius and Walther, 1991, 1992; Rosso and Rimstidt, 2000; Pokrovsky and Schott, 2000a, b; Kobayashi et al., 2001; Olsson et al., 2012; Martinez et al., 2014). Alkaline pH conditions (pH > 8.5) were proposed to favour the release of H_4SiO_4 from olivine (Pokrovsky and Schott, 2000a; Martinez et al., 2014). Under these conditions, the rate of H_4SiO_4 release would be controlled by the diffusion of reactive species (e.g. H^+, Na^+) through a Si depleted brucite-like layer of constant thickness (Wogelius and Walther, 1992; Pokrovsky and Schott, 2000a,b; Golubev et al., 2005). The extent to which each of these mechanisms controls olivine dissolution rates depends on pH and ionic strength (Pokrovsky and Schott, 2000a,b; Oelkers, 2001; Oelkers et al., 2009; Schott et al., 2009, 2012; Martinez et al., 2014). Further works have also proposed a steady-state long term dissolution rate, controlled by the removal of Mg and SiO_4^{4-} from the mineral active layer. This mechanism may lead to stoichiometric dissolution of olivine and a negligibly thin or absent Si-rich layer (Rimstidt et al., 2012; Maher et al., 2016).

In the presence of organic matter, however, the dissolution rate of olivine can be altered significantly (Grandstaff, 1986; Wogelius and Walther, 1991). For example, the bidentate or monodentate binding of organic ligands, and the interaction of bacteria biomass functional groups with Mg active sites on the mineral's surface can account for the enhancement or the inhibition of olivine dissolution, as a function pH (Wogelius and Walther, 1991; Pokrovsky et al., 2005; Golubev and Pokrovsky, 2006; Golubev et al., 2005; Shirokova et al., 2012; Hartmann et al., 2013; Declercq et al., 2013; Bundeleva et al., 2014; Oelkers et al., 2015). Liu et al. (2006) showed the enhancement of olivine dissolution at acidic pH values, in the presence of oxalic acid. However, a significant number of studies have shown decreases of up to 2 to 3 orders of magnitude in forsterite dissolution rates, in the presence of: (1) common freshwater bacteria, e.g. *Proteobacterium* (Garcia et al., 2013) and (2) solutions containing lysis products from dead organic matter and bacterial cell debris (Shirokova et al., 2012). Consequently, the interaction of active microbial communities, biofilm EPS, inert cell bacteria material, organic exudates, and humic acids may play a crucial role in the slow-down of Mg release from olivine, considerably inhibiting CO_2 sequestration by enhanced weathering, at the near-neutral pH values encountered

under natural conditions. These results may well be represented at the land's surface natural conditions (Spain et al., 2009; Rohini-Kumar et al., 2012).

As described previously, enhanced weathering methods would benefit from olivine dissolution on the Earth's surface as Mg^{2+} release is expected to promote CO_2 sequestration through the formation of Mg-carbonate minerals. To date, little experimental evidence exists to account for the expected weathering rates of fine powdered olivine artificially spread on the land's surface or for the capacity of this process to enhance CO_2 sequestration. As olivine powder will most likely come into contact with surface organic matter in aquatic environments, laboratory experiments herein, have taken inert biomass of *Synechococcus* sp. into consideration as a proxy for complex surface organic matter, to quantify its effects on the weathering rates of dispersed olivine. Inert organic matter at the pH of natural aqueous solutions, may affect enhanced weathering by (1) complexing Mg active sites on the dissolving olivine surface, and (2) decrease the rate of dissolution through pH buffering to alkaline conditions. In this study, the rates of olivine dissolution were quantified in partially closed batch reactors set ups described earlier in Martinez et al. (2014). As a source of dissolved CO_2 and maintain a constant pH value from which the rates can be derived and to avoid the use of inorganic buffers such as phosphates which may affect mineral dissolution rates, air was bubbled in experimental solutions at a constant rate of 3L/min in the presence of inert cyanobacteria biomass. This study contributes to closing the knowledge gaps concerning the interaction of inert organics and bacteria biomass with primary silicate dissolution mechanisms for the purpose of enhancing CO_2 sequestration within the realm of enhanced weathering.

2. Materials and Methods

The natural olivine used in this study represents a solid solution of its two end-members forsterite (Fo - Mg_2SiO_4) and fayalite (Fa - Fe_2SiO_4). The mineral was collected from an active quarry in Åheim, Norway. It is representative of a dunitic mantle rock and contains a $Fo_{89} – Fa_{11}$ component. For detailed information concerning the chemical composition of the natural olivine, the reader is referred to a previous study by Martinez et al. (2014). Prior to the crushing process,

the exposed reddish weathering crust of the dunite hand specimens was removed to avoid the effects of natural alteration. For kinetic experiments, the remaining olivine was crushed and sieved to a size of 40-63 μm. Other Mg rich minerals, such as enstatite ($Mg_2Si_2O_6$), occur in dunitic mantle rocks, however, their contribution to the release of Mg^{2+} and H_4SiO_4 is expected to be below detection limits. The olivine powder was cleaned with 100% ethanol to remove fine particles. The sample was dried at 65 °C overnight to a constant weight and then used for experiments. The specific surface area of the olivine powder was estimated with a particle sizer (Mastersizer MALVERN Instruments®) to be 0.1239 m^2/g. Scanning electron microscopy (SEM) was used to identify apparent dissolution features on olivine powder exposed to solutions containing inert biomass, with a LEO 1525 Field emission Oxford SEM/ EBSD system, at the University of Freiburg.

2.1 Preparation of inert cyanobacteria biomass for olivine dissolution experiments

The photosynthetic microorganism *Synechococcus* sp. (PCC 7942) is a unicellular coccoid cyanobacteria, containing outermost surface layers (S-layers), but no cell covering sheath (Martinez et al., 2008, 2010). Stock cultures of *Synechococcus* sp. were grown in BG-11 freshwater medium (Sigma–Aldrich C3061) for 2 weeks to the stationary phase. These cultures were kept at 22 ± 1 °C, under a 5000 lux cool-white fluorescent light illumination, and a constant humidified air flow delivered by an aquarium pump at 3L/min. After 15 days, 150 mL of *Synechococcus* sp. stock were transferred to an acid-washed and autoclaved 250-mL glass Schott® bottle and autoclaved at 121 °C for 20 minutes. Three 45 mL portions of this inert biomass solution were distributed into three sterile 50 mL Falcon® centrifuge tubes and centrifuged for 10 min at 13000 *x* g with a high speed centrifuge (Eppendorf® 5804). The supernatant was discarded and the remaining pellets were re-suspended and rinsed in 25 mL of sterile ultra-pure water (UPW). The centrifugation process was repeated two more times, with UPW and with sterile solutions of 0.001, 0.01 or 0.1 M $NaNO_3$. After the washing procedure, the remaining wet cell pellets were re-suspended in 45 mL of the appropriate background electrolyte and added to the partially closed reactors (Fig. 1) for olivine dissolution experiments. Heat treated cells have been shown to maintain their cellular structure intact as indicated previously (Wightman and Fein, 2004; Martinez et al., 2008, 2010; Bundeleva et al., 2014). The use of the complex inert biomass of cyanobacteria, representative of natural organic matter, allowed

quantification of olivine dissolution rates within the narrow near-neutral pH range of natural waters (6 < pH < 8) in the absence of growth or metabolic activity.

2.2 Acid base titration of inert Synechococcus sp. biomass

A volume of 200 mL of stock Synechococcus sp. cyanobacteria culture, grown to the stationary phase, was autoclaved for 20 minutes at 121ºC to generate inert biomass for acid base titration experiments. Aliquots of 50 mL of inert bacteria culture prepared for these experiments as indicated by Martinez et al. (2002). Prior to the start of acid base titration experiments, aliquots of background electrolyte solution containing the inert biomass were acidified to a pH of 3.0 with 4 µL of a 70% HNO3 stock solution (Sigma-Aldrich® 438073 ACS reagent). Titration of the inert biomass aliquots was performed with an automatic titrator system (Metrohm® Titrino 719S) as explained previously in Martinez et al. (2002). The resulting acid base titration data (i.e. volume of 0.1 M NaOH added vs pH) was analyzed with a Langmuir isotherm model and a linear programming optimization routine as explained previously (Martinez et al., 2002).

2.3 Partially-closed reactors systems

The term: “partially closed” was introduced previously by Martinez et al. (2014), and is reiterated here to describe modified closed batch reactors to which air is constantly injected at 3L/min using an aquarium pump (Marina 200® Hagen Deutschland GmbH & Co., Holm) connected to a gas (air) wash bottle to avoid evaporation of the reactor solution. These reactors are, however, closed with respect to the constant input of background electrolyte solution, but are considered to contain a permanent and, for the time frame of this study, an unlimited and constant contribution of Mg^{2+} and H_4SiO_4 from the dissolving olivine. The monitoring of [Mg^{2+}], [H_4SiO_4], pH and alkalinity in partially closed reactors, is expected to provide the information necessary to quantify olivine dissolution kinetics in the presence of inert biomass. Inorganic control reactors, containing 4g of olivine in an initial volume of 1L and under constant air injection, at 0.001, 0.01 or 0.1 M $NaNO_3$ were prepared. The washed dead cyanobacteria 45 mL aliquots were introduced into a second set of reactors with the same electrolyte conditions.

Sample aliquots of 30 mL were taken *in situ* at regular intervals from each partially closed reactor, to monitor the evolution of bulk solution parameters, to a maximum of 429 hours. The olivine powder and the inert cyanobacteria biomass were added simultaneously along with the start of air injection at a time zero for all reactors. These were first sampled after a period of 24 hours (Table 1). The reactors were placed in a water bath at a constant temperature of 22 ± 1 °C, as temperature changes have a significant effect on olivine dissolution rates (Wogelius and Walther, 1991; Awad et al., 2000; Oelkers, 2001). Mixing of the solution inside the reactors was achieved through the constant air flow. The olivine powder remained at the bottom of the reactor for the duration of the experiments. No suspended mineral particles were observed. At the end of the experimental runs the olivine powder was characterised with SEM as shown in Fig. 7.

2.4 Chemical analyses of sampled partially-closed reactor aliquots

The pH, the solution conductivity and the total alkalinity were determined for all sampled aliquots. In presence of inert cyanobacteria biomass, these parameters were measured without filtration. The pH in all samples was measured using a Metrohm® 6.0257.000 electrode, calibrated with of pH 4.01±0.01, 6.86 ±0.01, and 9.01±0.01 NIST standard buffers (CertiPUR® Buffer Solutions – Merck KGaA, Darmstadt, Germany). The total alkalinity was determined by titration with 0.1 M HCl using an automated titrator system (Metrohm® 719S Titrino). The conductivity was measured with a Metrohm® 6.0912.110 probe calibrated with a 100 µS/cm standard (Metrohm® 6.2324.010) and attached to a Metrohm® 712 Conductometer. Each sampled 30 mL aliquot was filtered through a N_2 degassed 0.22 µm cellulose acetate filter (Sartorius Stedim Biotech GmbH, Göttingen, Germany). The filtrate was analyzed for Mg concentration using a flame atomic absorption spectrometer (F-AAS Vario 6 Analytik Jena®) with a detection limit of >0.01 ppm. H_4SiO_4 concentrations were quantified by measuring the absorbance at 810 nm as described by the standard: "Deutsche Norm – DIN 38 405 - October 1990", using a Lambda 40 UV/VIS spectrometer (Perkin Elmer Instruments®) controlled by UV WinLab software®. This method had a detection limit of 0.2 ppm (0.003 mM).

2.5 Modeling of olivine dissolution rates

Results of Mg^{2+} and H_4SiO_4 release from olivine in 0, 0.001, 0.01 and 0.1 $NaNO_3$ both with and without inert cyanobacteria biomass are presented in Table 1. Concentrations of both of these species are quasi-linearly increasing over time for all experimental conditions, coinciding with previous studies for wollastonite (Pokrovsky et al., 2009). Considering that all solutions are undersaturated with respect to olivine, it has to be assumed that the changing Mg^{2+} and H_4SiO_4 concentrations have no effect on the olivine forward dissolution rate modelling, as indicated earlier by Pokrovsky et al. (2009). Under these conditions, the far-from equilibrium dissolution rates can be quantified for each individual experimental setting using the model equation below:

$$R = (d[Mg^{2+}]/dt)/SA \qquad (1)$$

here $d[Mg^{2+}]/dt$ stands for the change in Mg^{2+} concentration over the time interval dt, SA refers to the specific surface area of the olivine powder, determined using a particle size measuring instrument (Mastersizer MALVERN Instrument®). SA was found to be 0.1239 m^2/g for a particle size ranging between 40-63 µm. The SA value is in good agreement with previous B.E.T. surface area measurements for olivine reported by Pokrovsky and Schott (2000a,b). The rates of olivine dissolution in the presence of inert biomass and under inorganic conditions were calculated from the evolution of Mg^{2+} concentrations (Eq. 1) and reported in Table 2.

3. Results and Discussion

Fig. 2a and b show the evolution of pH as a function of time in partially-closed batch reactors under inorganic conditions and in the presence of inert cyanobacteria biomass respectively at background electrolyte levels ranging from 0 to 0.1 M $NaNO_3$. Experiments in the presence of olivine alone lie within a pH interval of 7.4 to 7.9, as observed previously for similar experimental conditions (Martinez et al., 2014). With added biomass, however, the solution pH ranged from 7.7 to 8.3. This increase in pH may be explained by the buffering of constantly dissolving CO_2 (H_2CO_3) by negatively charged *Synechococcus* sp. inert biomass surface functional groups ($R\text{-}L_B^-$). The presence a negative charge on the inert *Synechococcus* sp. biomass was shown in previous studies for the pH range of 3 to 11 (Martinez et al., 2008, 2010). From acid base titration data analysis of the inert biomass in this study, pK_a values of 5.2 ± 0.5,

6.9 ± 0.5 and 9.3 ± 0.5 with corresponding site concentrations of 0.39, 0.44 and 0.33 µmol/mg were obtained. These results confirm the development of a net negative charge within the pH range herein (7.5 < pH < 8.3), resulting from surface functional group deprotonation. A wealth of studies concerned with the characterization of the acid base properties of Gram negative bacteria surfaces, assign the first two most acidic pK_a values mentioned above, to carboxyl ($>COO^-$) and phosphoryl ($>PO_4^{2-}$) cell surface reactive sites (Fein et al., 1997; Daughney and Fein, 1998; Cox et al., 1999; Martinez et al., 2002, 2016; Ngwenya et al., 2003; Borrok and Fein, 2005; Claessens et al., 2006; Dittrich and Sibler, 2006; Pokrovsky et al., 2008, 2014). These groups may: (1) complex Mg active sites on the mineral surface to weaken >Mg-O bonds and, (2) buffer H_2CO_3 to bicarbonate (HCO_3) generating the moderate increase in pH and total alkalinity observed in Fig. 2 and 3, as explained in detail below.

Although difficult to constrain, as protons may be distributed between mineral surface sites or adsorbed to its surface layers, it is generally accepted that the dissolution of olivine depends on pH (Wogelius and Walther, 1991; Pokrovsky and Schott, 2000a,b; Oelkers, 2001; Pokrovsky et al., 2009; Martinez et al., 2014; Maher et al., 2016). At 0 M $NaNO_3$ and in the absence of organics, near-neutral pH conditions were generated by air bubbling. As described by the mechanism in Eqs. 2 to 4 below, constantly dissolving CO_2 rapidly equilibrates to HCO_3^- (to generate the total alkalinity) and H_3O^+ (the hydronium ion), where the latter species can promote olivine dissolution through protonation, leading to an increase in Mg^{2+} concentration and total alkalinity over time:

$$2H_2CO_3 + 2H_2O \rightarrow 2HCO_3^- + 2H_3O^+ \quad (2)$$

$$2H_3O^+ + >Mg_2SiO_4 \rightarrow 2[>Mg\text{-}OH_2^+] + >SiO_4H_2^0 \quad (3)$$

$$2H_2CO_3 + 2H_2O + >Mg_2SiO_4 \rightarrow 2HCO_3^- + 2[>Mg\text{-}OH_2^+] + >SiO_4H_2^0 \quad (4)$$

With inert biomass, the pH raises to a slightly alkaline average of 8.1 ± 0.1, compared to a mean value of 7.7 ± 0.1 under inorganic conditions, with a corresponding further increase in total alkalinity (Figs. 2 and 3). These results may be attributed to the additional buffering of H_2CO_3 by the deprotonated (negatively charged) inert cyanobacteria functional groups ($R\text{-}L_B^-$) as proposed below:

$$R\text{-}L_B^- + H_2CO_3 \rightarrow R\text{-}L_BH + HCO_3^- \qquad (5)$$

Under similar solution conditions (e.g. no $NaNO_3$ added), inert biomass functional groups may induce olivine dissolution. In Eq. 5 above, $R\text{-}L_B^-$ represents a functional group on the inert biomass surface, whose reactive nature may be compared to that of simpler dissolved organic ligands. As mentioned earlier, Liu et al. (2006) showed that oxalic acid promotes olivine dissolution at acidic pH (i.e. pH < 2). However, for near-neutral pH values, a number of laboratory and field studies have reported that organic ligands have a significant effect in mineral dissolution rates (Wogelius and Walther, 1991; Pokrovsky et al., 2009; Oelkers et al., 2015). Organic molecules showing complex structures, such as potassium hydrogen phthalate (KHP) and ascorbate can form organo-metallic complexes with the olivine surface Mg sites. These electropositive Mg atoms attract deprotonated (negatively charged) organic ligands from solution, leading to further polarization and weakening of the olivine >Mg-O bond allowing Mg organic ligand complex desorption (Wogelius and Walther, 1991; Oelkers, 2001; Schott et al., 2009; Pokrovsky and Schott, 2000a,b). In the presence of inert cyanobacteria biomass, functional groups, denoted by $R\text{-}L_B^-$, may show a similar behaviour on the mineral surface, such that:

$$2R\text{-}L_BH + >Mg_2SiO_4 \rightarrow 2[>Mg\text{-}L_B\text{-}R]^0 + >SiO_4H_2{}^0 \qquad (6)$$

where a biomass-Mg complex, $[>Mg\text{-}L_B\text{-}R]$, can form to weaken olivine Mg-O bonds and desorb Mg. In the absence of $NaNO_3$, the reaction in Eq. 6 is supported by the increase in Mg^{2+} concentration with respect to inorganic conditions, for experiments in the presence of inert biomass (Fig. 4a and b).

In the following paragraphs the influence of $NaNO_3$ on olivine dissolution will be discussed for the inorganic conditions and inert biomass experiments. As suggested earlier, H_2CO_3 buffering induces dissolution of olivine through protonation (Eqs. 2-4), as shown in previous works with similar experimental set-ups (Martinez et al., 2014). At near-neutral or slightly alkaline pH conditions, a negligibly thin Si-rich, Mg-depleted layer may be expected on the olivine surface as described by Pokrovsky and Schott (2000b) and Shirokova et al. (2012).

With raising Na^+ levels more dissolved Mg^{2+} is observed (Fig. 4), suggesting that in the near absence of a Si-rich layer on the olivine surface, Na^+ ions could enhance the generation of H_3O^+ for protonation of the mineral surface, through the mechanism in Eq. 7 under constant air injection (Martinez et al., 2014):

$$H_2O + Na^+ + H_2CO_3 \rightarrow NaHCO_3\ (aq) + H_3O^+ \qquad (7)$$

The above reaction leads to a larger extent of Mg^{2+}/H^+ exchange through protonation as a function of increasing $NaNO_3$ concentration. The mechanism in Eq. 7 is supported by the results in Fig. 4a, where at highest $NaNO_3$ values of 0.1 M, maximum Mg^{2+} concentrations of 0.53 mM were attained at the end of experiments. In addition, this reaction is further reinforced by the raise in total alkalinity observed in Fig. 3a, for the inorganic experiments, where the 0.1 M Na^+ condition shows the highest total alkalinity.

In the presence of inert biomass, Mg^{2+} concentrations extending from 0.15 to 0.40 mM were recorded at 0.1 M Na^+. The decrease in Mg^{2+} with respect to inorganic conditions in Fig. 4b implies an interaction of Na^+ with the $R\text{-}L_B^-$ species in Eq. 5. This would further lead to a decrease in total alkalinity with inert biomass, as shown for the 0.1 M Na^+ condition in Fig. 3b. Within experimental error the interaction of Na^+ with $R\text{-}L_B^-$ species would be further supported by the gradual reduction of the alkalinity at 0.001 and 0.01 M Na^+ in Fig. 3b, and the marked decrease in pH at 0.1 M Na^+ with respect to the 0 M $NaNO_3$ inert biomass experiments. Within the realm of enhanced weathering, the experimental results of this study indicate a negative combined effect of inert biomass and high $NaNO_3$ concentration on the process of Mg^{2+} release from the olivine surface, in natural aquatic systems, including soils, as well as freshwater and marine environments. This would suggest reduced carbonation of olivine powder, if dispersed on the Earth's surface, therefore leading to a lower capacity of this mineral to sequester CO_2.

Fig. 5 shows a continuous increase in silica concentration as a function of time. However, as apparent from this results and as shown in earlier works (Bennett et al., 1988), no significant difference in silica concentrations were observed between organic and inorganic data sets for all $NaNO_3$ concentrations (Fig. 5a and b), implying that neither Na^+ nor organic matter significantly

affected the mechanism of Si release form the olivine surface. From the evolution of Mg^{2+} and H_4SiO_4 concentrations, Mg/ H_4SiO_4 ratios of 2.1 ± 0.1 and 1.9 ± 0.3 were obtained from inorganic and inert biomass data sets respectively (Fig. 6a and b). These values reflect, within error, a long term stoichiometric dissolution behaviour within the near-neutral to slightly alkaline pH range of the experiments in this study. This finding is consistent with previous works which showed that olivine, apart from brief periods of incongruent dissolution, dissolves stoichiometrically under conditions similar to those herein (Pokrovsky and Schott, 2000a, b; Oelkers, 2001; Rimstidt et al. 2012; Shirokova et al., 2012). This results further suggest a steady state long term dissolution rate, controlled by the net removal of Mg and H_4SiO_4 from the mineral active layer (Maher et al., 2016), and a negligibly thin or absent Si-rich layer upon olivine dissolutions.

SEM images in Fig. 7a and b show the surface features of the previously crushed but unreacted olivine powder, caused by exposure to solutions containing inert biomass. Under these conditions, and at 0.01 $NaNO_3$ olivine grains show etch pits with different morphological characteristics. These include, random sized, elongated etched surface structures and rounded, conical surface pits comparable to those formed by simple organic ligands (e.g. catechol) and humic acids as shown previously by Pokrovsky et al. (2009) and Oelkers et al. (2015). The different forms of etch pits on the olivine in this study, may suggest the interaction of inert biomass ligands with the mineral surface to generate the different morphological features of the etch pits. This coincides with SEM imaging studies reporting etch pits formed by biotic natural weathering, which are non-uniform in size for an individual sample (Velbel, 2009).

Fig. 8 shows a combined plot of the rates of olivine dissolution under inorganic conditions and in the presence of inert cyanobacteria biomass. In order to determine whether a statistically significant difference was present between these values, the Saphiro-Wilk Test, or W test for normality, was used as indicated earlier (Shapiro and Wilk, 1965 a, b; Rimstidt et al., 2012). This method is particularly well suited for small sized datasets of $n < 50$ and relies on the Shapiro Wilk test coefficient tables (Shapiro and Wilk, 1965 a, b). From all the rate data shown in table 2 and Fig. 8, 25 values were selected from each the inorganic and inert biomass conditions, each with a total of 39 data points, for a combined total of 50 points. This newly

generated data set was arranged in ascending order (i.e. from lowest to highest values). Prior to selection of the 25 data points required for the Shapiro-Wilk test, values that fell beyond the 3σ standard deviation were discarded from the mean of the original 39 data points (Rimstidt et al., 2012). Corresponding to each of the Shapiro Wilk test coefficients for i = 1…n, where n = 50, the difference, d, between highest and lowest values in the 50 point data set was calculated. The d value was determined such that for the i^{th} pair, $d = x_{(n+1-i)}-x_i$, with $x_{(n+1-i)}$ being the highest value and x_i the lowest value. Subsequently, the resulting d values were multiplied by their respective Shapiro Wilk test coefficients (c) and the resulting values were added up. This sum, b, can be defined as:

$$b = \sum_{i=1}^{n} c_i * \left[x_{(n+1-i)} - x_i\right] \quad (8)$$

The overall average from all 50 data points was calculated, $\bar{x}$, then each value in the dataset was substracted from the average, and the result was squared. This is defined as the sum of the squares, *SS*:

$$SS = \sum_{i=1}^{n} (\bar{x} - x_i)^2 \quad (9)$$

According to Shapiro and Wilk (1965a,b) and as suggested in Rimstidt et al., (2012), the W test statistic, W can be defined such that:

$$W = b^2/SS \quad (10)$$

where, in this study the W statistic had a value of 0.94 which for n = 50 corresponds to a p value greater than 0.03, suggesting a normal distribution of the selected dissolution rate data. This implies that no significant differences exist between the rates calculated under inorganic conditions or in the presence of inert biomass. These results, further suggest no influence of dead cyanobacteria biomass on the rates of olivine dissolution under the experimental conditions herein. This is also consistent with the results of previous studies showing no effect of a suite of organic ligands on primary silicate mineral dissolution, except at their exceptionally high concentrations, not relevant to natural settings (Wogelius and Walther, 1991; Pokrovsky et al., 2009). From the perspective of enhanced weathering processes, a negative effect of organic matter would be exerted on the efficiency of CO_2 mineralization in the presence of dissolving primary silicates artificially dispersed on the Earth's surface.

4. Conclusion

This study was concerned with quantifying the rates of olivine dissolution with inert biomass to account for its effects CO_2 mineralization, within the context of enhanced weathering processes. However, the results of this work showed that inert biomass does not influence the rates of olivine dissolution as no significant differences were found with respect to the inorganic conditions. This suggests that the presence of organic matter will lead to a decreased effect of the carbonation processes needed for CO_2 sequestration by primary silicates. Further research needs to be conducted in order to improve the use of abundant primary silicate minerals for carbonate formation. It is also important to note that apart from Mg^{2+}, other metallic elements such as Ni and Cr are present in the olivine structure. These latter elements can be toxic and this generates a source of concern regarding the application of enhanced weathering. This secondary effects should be taken into account if a global enhanced weathering strategy is to be implemented without alteration of biogeochemical processes within the Earth's critical zone.

Acknowledgments

Funding for this research project was provided by a research grant from Science Support Center (SSC) Research Innovations Fund from the University of Freiburg to REM (Innovationsfonds Forschung Kapitel: 1410, TG 99, BA 600,197). The authors would like to thank Dr. Eric H. Oelkers of the GET-CNRS in Toulouse, France, for helpful comments during the preparation of this manuscript. Furthermore, the authors are grateful to Dr. Andreas Danilewsky of the Crystallography Department at the University of Freiburg, for help with SEM imaging. In addition the authors would like to thank Nataliya Paunova and Sigrid Hirth-Walther of the Institute for Earth and Environmental Science at the University of Freiburg for sample analysis.

Figure Captions

Figure 1. One liter partially closed batch reactor set-ups for quantifying the rates of olivine mineral dissolution under inorganic conditions and in the presence of inert *Synechococcus* sp. biomass under continuous CO_2 bubbling.

Figure 2. Monitoring of pH in partially closed batch reactors as a function of time. Circle, triangle, square and diamond markers correspond to ionic strengths of 0, 0.001, 0.01 and 0.1 M $NaNO_3$ respectively. Filled symbols correspond to experiments under inorganic conditions (●,▲, ■, ◆) and the open symbols describe results for experiments containing inert *Synechococcus* sp. biomass (○, Δ, □, ◇).

Figure 3. Monitoring of Mg concentration in partially closed batch reactors as a function of time. Circle, triangle, square and diamond markers correspond to ionic strengths of 0, 0.001, 0.01 and 0.1 M $NaNO_3$ respectively. Filled symbols correspond to experiments under inorganic conditions (●,▲, ■,◆) and the open symbols describe results for experiments containing inert *Synechococcus* sp. biomass (○, Δ, □, ◇).

Figure 4. Monitoring of alkalinity in partially closed batch reactors as a function of time. Circle, triangle, square and diamond markers correspond to ionic strengths of 0, 0.001, 0.01 and 0.1 M $NaNO_3$ respectively. Filled symbols correspond to experiments under inorganic conditions (●,▲, ■, ◆) and the open symbols describe results for experiments containing inert *Synechococcus* sp. biomass (○, Δ, □, ◇).

Figure 5. Monitoring of alkalinity in partially closed batch reactors as a function of time. Circle, triangle, square and diamond markers correspond to ionic strengths of 0, 0.001, 0.01 and 0.1 M $NaNO_3$ respectively. Filled symbols correspond to experiments under inorganic conditions (●,▲, ■, ◆) and the open symbols describe results for experiments containing inert *Synechococcus* sp. biomass (○, Δ, □, ◇).

Figure 6. Plot of Mg/Si ratios as a function of pH. Circle, triangle, square and diamond markers correspond to ionic strengths of 0, 0.001, 0.01 and 0.1 M $NaNO_3$ respectively. Filled symbols correspond to experiments under inorganic conditions (●,▲, ■, ◆) and the open symbols describe results for experiments containing inert Synechococcus sp. biomass (○, Δ, □, ◇).

Figure 7. SEM photomicrographs of the reacted olivine powder from inert biomass experiment runs, showing surface pits on the olivine surface, which may be related to the presence of organic acids.

Figure 8. Plot of the log of the rate of olivine dissolution (log R_{OL}) calculated by Eq. (1) as a function of pH. Filled symbols correspond to experiments under inorganic conditions (●,▲, ■, ◆) and the open symbols describe results for experiments containing inert *Synechococcus* sp. biomass (○, Δ, □, ◇).

References

Alexander, G., Maroto-Valer, M.M., Gafarova-Aksoy, P., 2007. Evaluation of reaction variables in the dissolution of serpentine for mineral carbonation. Fuel 86, 273–281.

Alfredsson, H.A., Hardarson, B.S., Franzson, H., Gislason, S.R., 2008. CO_2 sequestration in basaltic rock at the Hellisheidi site in SW Iceland: stratigraphy and chemical composition of the rocks at the injection site. Mineral. Mag. 72, 1-5.

Aradóttir, E.S.P., Sonnenthal, E.L., Jónsson, H., 2012. Development and evaluation of a thermodynamic dataset for phases of interest in CO_2 mineral sequestration in basaltic rocks. Chem. Geol. 304-305, 26–38.

Awad, A., Koster van Groos, A.F., Guggenheim, S., 2000. Forsteritic olivine: effect of crystallographic direction on dissolution kinetics. Geochim. Cosmochim Acta. 64, 1765–1772.

Bachu, S., Adams, J.J., 2003. Sequestration of CO_2 in geological media in response to climate change: capacity of deep saline aquifers to sequester CO_2 in solution. Energ. Convers. Manage. 44, 3151–3175.

Bachu, S, 2008. CO_2 storage in geological media: Role, means, status and barriers to deployment. Prog. Energ. Combust. 34, 254-273.

Bennett, P.C., Melcer, M.E., Siegel, D.I., Hassett, J.P., 1988. The dissolution of quartz in dilute aqueous solutions of organic acids at 25 °C. Geochim. Cosmochim Acta. 52, 1521 – 1530.

Berner, R.A., Lasaga, A.C., Garreis, R.M., 1983. The carbonate-Silicate Geochemical cycle and its effect on atmospheric carbon dioxide over the past 100 million years. Am. J. Sci. 283, 641-683.

Borrok, D., Turner, B.F., Fein, J.B., 2005. Universal surface complexation framework for modeling proton binding onto bacterial surfaces in geologic settings. Am. J. Sci. 305, 826–853.

Bundeleva, I.A., Menez, B., Augé, T., Bodénan, F., Recham, N., Guyot, F., 2014. Effects of cyanobacteria Synechococcus PCC 7942 on carbonation kinetics of olivine at 20 °C. Miner. Eng. 59, 2-11.

Casey, W.H., Westrich, H., 1992. Control of dissolution rates of orthosilicate minerals by divalent metal–oxygen bonds. Nature 355, 157–159.

Claessens, J., van Lith, Y., Laverman, A.M., Van Cappellen, P., 2006. Acid–base activity of live bacteria: implications for quantifying cell wall charge. Geochim. Cosmochim. Acta 70, 267–276.

Cox, J.S., Smith, D.S., Warren, L.A., Ferris, F.G., 1999. Characterizing heterogeneous bacterial surface functional groups using discrete affinity spectrum for proton binding. Environ. Sci. Technol. 33, 4514–4521.

Daughney, C.J., Fein, J.B. Yee. N., 1998. A comparison of the thermodynamics of metal adsorption onto two common bacteria. Chem. Geol. 144, 161–176.

Declercq, J., Bosc, O., Oelkers E.H., 2013. Do organic ligands affect forsterite dissolution rates? Appl Geochem. 39, 69–77.

Dittrich, M., Sibler, S., 2006. Influence of H^+ and calcium ions on surface functional groups of synechococcus PCC 7942 cells. Langmuir 22, 5435–5442.

Dufaud, F., Martinez, I., Shilobreeva, S., 2009. Experimental study of Mg-rich silicates carbonation at 400 and 500 °C and 1 kbar. Chem. Geol. 265, 79–87.

Eikeland, E., Blichfeld, A.B., Tyrsted, C., Jensen, A., Iversen, B.B., 2015. Optimized Carbonation of magnesium Silicate Mineral for CO2 Storage. Appl. Mater. Inter. 7, 5258 – 5264.

Fein, J.B., Daughney, C.J., Yee, N., Davis, T.A., 1997. A chemical equilibrium model for metal adsorption onto bacterial surfaces. Geochim. Cosmochim. Acta 61, 3319–3328.

Ferris, F.G., Wiese, R.G., Fyfe, W.S., 1994. Precipitation of carbonate minerals by microorganisms: Implications for silicate weathering and the global carbon dioxide budget. Geomicrobiol. J. 12, 1–13.

Garcia, B., Lemelle, L., Rose-Koga, E., Perriat, P., Basset, R., Gillet, P., Albarède, F., 2013. An experimental model approach of biologically-assisted silicate dissolution with olivine and Escherichia coli – Impact on chemical weathering of mafic rocks and atmospheric CO_2 drawdown. Appl. Geochem. 31, 216–227.

Garcia, B., Beaumont, V., Perfetti, E., Rouchon, V., Blanchet, D., Oger, P., Dromart, G., Huc, A.Y., Haeseler, F., 2010. Experiments and geochemical modelling of CO_2 Sequestration by olivine: Potential, quantification. Appl. Geochem. 25, 1383-1396.

Gerdemann, S.J., O'Connor, W.K., Dahlin, D.C., Penner, L.R., Rush, H., 2007. Ex Situ Aqueous Mineral Carbonation. Environ. Sci. Technol., 41, 2587–2593.

Giammar, D.E., Bruant, R.G., Peters, C.A., 2005. Forsterite dissolution and magnesite precipitation at conditions relevant for deep saline aquifer storage and sequestration of carbon dioxide. Chem. Geol. 217, 257–276.

Gislason, S.R., Wolff-Boenisch, D., Stefansson, A., Oelkers, E.H., Gunnlaugsson, E., Sigurdardottir, H., Sigfusson, B., Broecker, W.S., Matter J.M., Stute, M., Axelsson, G., Fridriksson, T., 2010. Mineral sequestration of carbon dioxide in basalt: A pre-injection overview of the CarbFix project. Int. J. Greenh. Gas Control 4, 537–545.

Gislason, S.R., Oelkers, E.H., 2014. Carbon Storage in Basalt, Science 344, 373 – 374.

Goff, F., Lackner, K.S., 1998. Carbon dioxide sequestering using ultramafic rocks. Environ. Geosci. 5, 89 – 101.

Golubev, S.V., Pokrovsky, O.S., Schott, J., 2005. Experimental determination of the effect of dissolved CO_2 on the dissolution kinetics of Mg and Ca silicates at 25 °C. Chem. Geol. 217, 227–238.

Golubev, S.V., Pokrovsky, O.S., 2006. Experimental study of the effect of organic ligands on diopside dissolution kinetics. Chem. Geol. 235, 377–389.

Golubev, S.V., Bauer, A., Pokrovsky, O.S., 2006. Effect of pH and organic ligands on the kinetics of smectite dissolution at 25 °C. Geochim. Cosmochim Acta. 70, 4436–4451.

Grandstaff, D.E., 1986. The dissolution rate of forsteritic olivine from Hawaiian beach sand. In Rates of Chemical Weathering of Rocks and Minerals (eds S. M. Colman and D. P. Dethier). 41 – 59, Academic Press, Inc.

Gysi, A.P., Stefánsson, A., 2012. Experiments and geochemical modeling of CO_2 sequestration during hydrothermal basalt alteration. Chem. Geol. 306–307, 10–28.

Hartmann, J., Jansen, N., Dürr, H.H., Kempe, S., Köhler, P., 2009. Global CO_2 consumption by chemical weathering: What is the contribution of highly active weathering regions? Global Planet. Change 69, 185–194.

Hartmann, J., West, A.J., Renforth, P., Köhler, P., De La Rocha, C.L., Wolf-Gladrow, D.A., Dürr, H.H., Scheffran, J., 2013. Enhanced chemical weathering as a geoengineering strategy to reduce atmospheric carbon dioxide, supply nutrients, and mitigate ocean acidification, Rev. Geophys. 51, 113–149.

Huijgen, W.J.J., Witkamp, G.J., Comans, R.N.J., 2006. Mechanisms of aqueous wollastonite carbonation as a possible CO_2 sequestration process. Chem. Eng. Sci., 61, 4242 - 4251.

Jia, L., Anthony, E.J., Lin, W., Ruan, Y., Gora, D., 2004. Carbonation of Magnesium Silicate Minerals: an Experimental Study. CJChE 82, 1289 1295.

Kelemen, P.B., Matter, J., Streit, E.E., Rudge, J.F., Curry, W.B., Blusztajn, J., 2011. Rates and Mechanisms of Mineral Carbonation in Peridotite: Natural Processes and Recipes for Enhanced, in situ CO_2 Capture and Storage. Ann. Rev. Earth Planetary Sci. 39, 545-576.

King, H.E., Plümper, O., Putnis, A., 2010. Effect of Secondary Phase Formation on the Carbonation of Olivine. Environ. Sci. Technol. 44, 6503–6509.

Klein, F., McCollom, T.M., 2013. From serpentinization to carbonation: New insights from a CO_2 injection experiment. Earth Planet Sc Lett 379, 137–145.

Kobayashi, M., Sawada, A., Tani, Y., Soma, M., Tanaka, A., Honma, T., Seyama, H., Theng, B. K.G., 2001. Acid Dissolution of Olivines, Feldspars and Dunite. Water Air Soil Poll. 130, 757–762.

Lackner, K.S., 2003. A guide to CO_2 sequestration. Science 300, 1677–1678.

Liu, Y., Olsen, A.A., Rimstidt, J.D., 2006. Mechanism for the dissolution of olivine series minerals in acidic solutions. Am Mineral 91, 455 – 458.

Maher, K., Johnson, N.C., Jackson, A., Lammers, L.N., Torchinsky, A.B., Weaver, K.L., Bird, D.K., Brown Jr., G.E., 2016. A spatially resolved surface kinetic model for forsterite dissolution. Geochim. Cosmochim. Acta 174, 313-334.

Martinez, R.E., Smith, D.S., Kulczycki, E., Ferris, F.G., 2002. Determination of Intrinsic Bacterial Surface Acidity Constants using a Donnan Shell Model and a Continuous pKa Distribution Method. J. Colloid Interface Sci. 253, 130–139.

Martinez, R.E., Pokrovsky, O.S., Schott, J., Oelkers, E.H., 2008. Surface charge and zeta-potential of metabolically active and dead cyanobacteria. J. Colloid Interface Sci. 323, 317–325.

Martinez, R.E., Gardès, E., Pokrovsky, O.S., Schott, J., Oelkers, E.H., 2010. Do photosynthetic bacteria have a protective mechanism against carbonate precipitation at their surfaces? Geochim. Cosmochim Acta. 74, 1329–1337.

Martinez, R.E., Weber, S., Bucher, K., 2014. Quantifying the kinetics of olivine dissolution in partially closed and closed batch reactor systems. Chem. Geol. 367, 1–12.

Matter J.M., Broecker, W.S., Gislason, S.R., Gunnlaugsson, E., Oelkers, E.H., Stute, M., Sigurdardóttir, H., Stefansson, A., Alfreðsson, H.A., Aradóttir, E.S., Axelsson, G. , Sigfússon, B.

Wolff-Boenisch, D., 2011. The CarbFix Pilot Project – Storing Carbon Dioxide in Basalt. Energy Procedia 4, 5579–5585.

Matter, J.M., Broecker, W.S., Stute, M., Gislason, S.R., Oelkers, E.H., Stefánsson, A., Wolff-Boenisch, D., Gunnlaugsson E., Axelsson G., and Björnsson G., 2009. Permanent Carbon Dioxide Storage into Basalt: The CarbFix Pilot Project, Iceland. Energy Procedia 1, 3641 – 3646.

McGrail, B.P., Schaef, H.T., Ho, A.M., Chien, Y.-J., Dooley, J.J., Davidson, C.L., 2006. Potential for carbon dioxide sequestration in flood basalts. J. Geophys. Res. 111, 1-13.

Ngwenya, B.T., Suthermand, I.W., Kennedy, L., 2003. Comparison of the acid–base behaviour and metal adsorption characteristics of a gram-negative bacterium with other strains. Appl. Geochem. 18, 527–538.

O'Connor, W.K., Dahlin, D.C., Rush, G.E., Dahlin, C.L., Collins, W.K., 2002. Carbon dioxide sequestration by direct mineral carbonation: Process mineralogy of feed and products, Miner. Metall. Processes 19, 95 – 101.

Oelkers E.H., Golubev, S.V., Chairat, C., Pokrovsky, O.S., Schott, J., 2009. The surface chemistry of multi-oxide silicates. Geochim. Cosmochim Acta. 73, 4617–4634.

Oelkers, E.H., 2001. An experimental study of forsterite dissolution rates as a function of temperature and aqueous Mg and Si concentrations. Chem. Geol. 175, 485–494.

Oelkers E.H., Schott, J., 2005. Geochemical aspects of CO_2 sequestration. Chem. Geol. 217, 183 – 186.

Oelkers, E.H., 2008. Mineral carbonation of CO_2. Elements, 4, 333.

Oelkers, E.H., Benning, L.G., Lutz, S., Mavromatis, V., Pearce, C.R., Plumper, O., 2015. The efficient long-term inhibition of forsterite dissolution by common soil bacteria and fungi at Earth surface conditions. Geochim. Cosmochim Acta. 168, 222–235.

Olsson, J., Bovet, N., Makovicky, E., Bechgaard, K., Balogh, Z., Stipp, S.L.S., 2012. Olivine reactivity with CO_2 and H_2O on a microscale: Implications for carbon sequestration. Geochim. Cosmochim Acta. 77, 86–97.

Orlando, A., Borrini, D., Marini, L., 2011. Dissolution and carbonation of a serpentinite: Inferences from acid attack and high P–T experiments performed in aqueous solutions at variable salinity. Appl. Geochem. 26, 1569–1583.

Oskierski, H.C., Dlugogorski B.Z., Jacobsen, G., 2013a. Sequestration of atmospheric CO_2 in chrysotile mine tailings of the Woodsreef Asbestos Mine, Australia: Quantitative mineralogy, isotopic fingerprinting and carbonation rates. Chem. Geol. 358, 156–169.

Oskierski, H.C., Dlugogorski B.Z., Jacobsen, G., 2013b. Sequestration of atmospheric CO_2 in a weathering-derived, serpentinite-hosted magnesite deposit: ^{14}C tracing of carbon sources and age constraints for a refined genetic model. Geochim. Cosmochim Acta. 122, 226–246.

Park, A.-H.A., Jadhav, R., Fan, L.-S., 2003. CO_2 Mineral Sequestration: Chemically Enhanced Aqueous Carbonation of Serpentine. CJChE 81, 885 – 890.

Park, A.-H.A., Fan, L.-S., 2004. CO_2 mineral sequestration: physically activated dissolution of serpentine and pH swing process. Chem. Eng. Sci. 59, 5241–5247.

Pokrovsky, O.S., Martinez, R., Golubev, S.V., Kompantseva, E.I., Shirokova, L.S., 2008. Adsorption of metals and protons on Gloeocapsa sp. cyanobacteria: a surface speciation approach. Appl. Geochem. 23, 2574–2588.

Pokrovsky, O.S., Schott, J., Castillo, A., 2005. Kinetics of brucite dissolution at 25 °C in the presence of organic and inorganic ligands and divalent metals. Geochim. Cosmochim. Acta 69, 905–918.

Pokrovskii, O.S. Schott, J., 2000a. Kinetics and mechanism of forsterite dissolution at 25 °C and pH from 1 to 12. Geochim. Cosmochim. Acta 64 , 3313 – 3325.

Pokrovsky, O. S., Schott, J. 2000b. Forsterite surface composition in aqueous solutions: a combined potentiometric, electrokinetic, and spectroscopic approach. Geochim. Cosmochim. Acta 64, 3299 – 3312.

Pokrovsky, O.S., Shirokova, L.S., Benezeth, P. , Schott, J., Golubev, S.V., 2009. Effects of organic ligands and heterotrophic bacteria on wollastonite dissolution kinetics. Am. J. Sci., 309, 731-772.

Pronost, J., Beaudoin, G., Tremblay, J., Larachi, F., Duchesne, J., Hébert, R., Constantin M., 2011. Carbon Sequestration Kinetic and Storage Capacity of Ultramafic Mining Waste. Environ. Sci. Technol. 45, 9413–9420.

Rimstidt, J.D., Brantley, S.L., Olsen, A.A., 2012. Systematic review of forsterite dissolution rate data. Geochim. Cosmochim. Acta 99, 159–178.

Rohini-Kumar, M., Osborne, J.W., Saravanan, V.S. 2012. Comparison of soil bacterial communities of Pinus patula of Nilgiris, Western Ghats with other biogeographical distinct pine forest clone libraries. Microb. Ecol. 66, 132–144.

Rosso, J.J. Rimstidt J.D., 2000. A high resolution study of forsterite dissolution rates. Geochim. Cosmochim. Acta 64, 3299–3312.

Schaefer, M., Behrendt, F., Hammer, T., 2010. Evaluation of strategies for the subsequent use of CO_2. Front. Chem. Eng. China 4, 172 -183.

Schott, J., Pokrovsky, O.S., Spalla, O., Devreux, F., Gloter, A., Mielczarski, J.A., 2012. Formation, growth and transformation of leached layers during silicate minerals dissolution: The example of wollastonite. Geochim. Cosmochim. Acta 98, 259–281

Schott, J., Pokrovsky, O.S., Oelkers, E.H., 2009. The Link Between Mineral Dissolution/Precipitation Kinetics and Solution Chemistry. Reviews in Mineral. and Geochem. 70, 207 – 258.

Schuiling, R.D., Krijgsman, P., 2006. Enhanced weathering: An effective and cheap tool to sequester CO_2. Clim. Change, 74, 349–354.

Shapiro, S.S., Wilk, M.B., 1965a. Testing the normality of several samples. (Unpublished manuscript).

Shapiro, S.S., Wilk, M.B., 1965b. An analysis of variance test for normality (incomplete samples). Biometrika, 52, 591-611.

Shirokova, L.S., Bénézeth, P., Pokrovsky, O.S., Gerard, E., Ménez B., Alfredsson H., 2012. Effect of the heterotrophic bacterium Pseudomonas reactans on olivine dissolution kinetics and implications for CO_2 storage in basalts. Geochim. Cosmochim. Acta 80, 30–50.

Spain, A.M., Krumkolz, L.R., Elshahed, M.S., 2009. Abundance, composition, diversity and novelty of soil Proteobacteria. ISME J. 3, 992–2000.

Velbel, M.A., 2009. Dissolution of olivine during natural weathering. Geochim. Cosmochim. Acta 73, 6098 – 6113.

Wightman, P.G., Fein, J.B. 2004. The effect of bacterial cell wall adsorption on mineral solubilities. Chem. Geol. 212, 247–254.

Wogelius, R.A., Walther, J.V., 1991. Olivine dissolution at 25°C: Effects of pH, CO_2, and organic acids, Geochim. Cosmochim. Acta 55, 943-954.

Wogelius, R.A., Walther, J.V., 1992. Olivine dissolution kinetics at near-surface conditions Chem. Geol. 97, 101–112.

Zhang, M., Bachu, S. 2011 Review of integrity of existing wells in relation to CO_2 geological storage: What do we know? Int. J. Greenh. Gas Control 5, 826–840.

Table 1. Summary of inorganic and organic experiment runs performed at 25 °C and 1 bar

Exp #	Time (hours)	pH	IS (M)	Biomass* (mg/L)	Alkalinity (mM)	Mg^{2+} (mM)	SiO_2(aq) (mM)	Mg/Si
1.1	0	N.D.	1.00×10^{-04}	0	0.080	N.D.	N.D.	
1.2	43	7.47	1.19×10^{-02}		0.590	1.186×10^{-01}	7.103×10^{-02}	1.67
1.3	69	7.65	1.15×10^{-02}		0.545	1.553×10^{-01}	7.111×10^{-02}	2.18
1.4	93	7.75	1.11×10^{-02}		0.550	1.692×10^{-01}	9.484×10^{-02}	1.78
1.5	165	7.79	1.07×10^{-02}		0.675	1.966×10^{-01}	1.050×10^{-01}	1.87
1.6	189	7.90	1.04×10^{-02}		0.715	2.055×10^{-01}	1.130×10^{-01}	1.82
1.7	213	7.81	9.99×10^{-03}		0.690	2.137×10^{-01}	8.031×10^{-02}	2.66
1.8	237	7.90	9.61×10^{-03}		0.745	2.203×10^{-01}	9.746×10^{-02}	2.26
1.9	261	7.91	9.24×10^{-03}		0.510	2.446×10^{-01}	8.473×10^{-02}	2.89
1.10	333	7.91	8.87×10^{-03}		0.726	2.659×10^{-01}	1.351×10^{-01}	1.97
1.11	357	7.93	8.49×10^{-03}		0.698	2.704×10^{-01}	1.466×10^{-01}	1.84
1.12	381	7.96	8.12×10^{-03}		0.675	2.720×10^{-01}	1.403×10^{-01}	1.94
2.1	0	5.14	1.00×10^{-04}	711 ± 24	0.310	N.D.	N.D.	
2.2	43	7.83	5.80×10^{-04}		0.895	1.829×10^{-01}	7.684×10^{-02}	2.38
2.3	69	7.98	6.93×10^{-04}		1.250	1.941×10^{-01}	8.334×10^{-02}	2.33
2.4	93	8.08	7.50×10^{-04}		1.145	2.314×10^{-01}	1.315×10^{-01}	1.76
2.5	165	8.10	9.71×10^{-04}		1.285	2.662×10^{-01}	1.216×10^{-01}	2.19
2.6	189	8.18	1.01×10^{-03}		1.250	2.803×10^{-01}	8.664×10^{-02}	3.24
2.7	213	8.16	1.07×10^{-03}		1.360	2.868×10^{-01}	9.133×10^{-02}	3.14
2.8	237	8.16	1.10×10^{-03}		1.315	3.060×10^{-01}	1.160×10^{-01}	2.64
2.9	261	8.19	1.10×10^{-03}		1.610	3.250×10^{-01}	1.935×10^{-01}	1.68
2.10	333	8.19	1.16×10^{-03}		1.485	3.425×10^{-01}	1.798×10^{-01}	1.91
2.11	357	8.19	1.18×10^{-03}		1.440	3.531×10^{-01}	1.934×10^{-01}	1.83
2.12	381	8.18	1.25×10^{-03}		2.055	3.589×10^{-01}	1.905×10^{-01}	1.88
3.1	0	5.43	4.76×10^{-04}	0	0.660	N.D.	N.D.	
3.2	43	7.51	8.70×10^{-04}		0.425	1.793×10^{-01}	7.811×10^{-02}	2.30

3.3	69	7.62	9.27×10^{-04}		0.625	1.985×10^{-01}	9.082×10^{-02}	2.19
3.4	93	7.75	9.67×10^{-04}		0.510	2.306×10^{-01}	1.456×10^{-01}	1.58
3.5	165	7.79	1.07×10^{-03}		0.590	2.639×10^{-01}	1.330×10^{-01}	1.98
3.6	189	7.85	1.11×10^{-03}		0.645	2.752×10^{-01}	1.201×10^{-01}	2.29
3.7	213	7.84	1.16×10^{-03}		0.655	2.848×10^{-01}	1.069×10^{-01}	2.66
3.8	237	7.85	1.15×10^{-03}		0.660	2.975×10^{-01}	1.339×10^{-01}	2.22
3.9	261	7.85	1.24×10^{-03}		0.650	3.249×10^{-01}	1.412×10^{-01}	2.30
3.10	333	7.86	1.22×10^{-03}		0.700	3.440×10^{-01}	1.556×10^{-01}	2.21
3.11	357	7.91	1.28×10^{-03}		0.710	3.509×10^{-01}	1.547×10^{-01}	2.27
3.12	381	7.93	1.35×10^{-03}		0.725	3.592×10^{-01}	1.808×10^{-01}	1.99
4.1	0	5.32	5.14×10^{-04}	724 ± 12	0.060	N.D.	N.D.	
4.2	43	7.90	1.86×10^{-03}		0.985	1.871×10^{-01}	1.180×10^{-01}	1.58
4.3	69	8.05	1.95×10^{-03}		1.215	2.185×10^{-01}	1.230×10^{-01}	1.78
4.4	93	8.05	2.07×10^{-03}		1.150	3.125×10^{-01}	2.117×10^{-01}	1.48
4.5	165	8.13	2.25×10^{-03}		1.345	3.079×10^{-01}	2.377×10^{-01}	1.30
4.6	189	8.16	2.54×10^{-03}		1.545	3.140×10^{-01}	1.752×10^{-01}	1.79
4.7	213	8.18	2.39×10^{-03}		1.395	3.276×10^{-01}	1.534×10^{-01}	2.14
4.8	237	8.20	2.38×10^{-03}		1.410	3.199×10^{-01}	1.549×10^{-01}	2.06
4.9	261	8.20	2.42×10^{-03}		1.430	3.668×10^{-01}	2.779×10^{-01}	1.32
4.10	333	8.18	2.44×10^{-03}		1.520	3.784×10^{-01}	2.197×10^{-01}	1.72
4.11	357	8.19	2.40×10^{-03}		1.410	3.755×10^{-01}	1.999×10^{-01}	1.88
4.12	381	8.21	2.48×10^{-03}		1.490	3.797×10^{-01}	2.051×10^{-01}	1.85
5.1	0	5.54	1.15×10^{-02}	0	0.080	N.D.	N.D.	
5.2	43	7.46	1.18×10^{-02}		0.490	1.862×10^{-01}	9.136×10^{-02}	2.04
5.3	69	7.63	1.17×10^{-02}		0.490	2.274×10^{-01}	9.720×10^{-02}	2.34
5.4	93	7.71	1.18×10^{-02}		0.550	2.697×10^{-01}	1.594×10^{-01}	1.69
5.5	165	7.83	1.18×10^{-02}		0.605	3.173×10^{-01}	1.482×10^{-01}	2.14
5.6	189	7.85	1.20×10^{-02}		0.660	3.364×10^{-01}	1.552×10^{-01}	2.17
5.7	213	7.86	1.21×10^{-02}		0.735	3.498×10^{-01}	1.721×10^{-01}	2.03

5.8	237	7.86	1.20×10^{-02}		0.745	3.665×10^{-01}	1.631×10^{-01}	2.25
5.9	261	7.85	1.23×10^{-02}		0.860	3.840×10^{-01}	1.582×10^{-01}	2.43
5.10	333	7.86	1.22×10^{-02}		0.815	4.151×10^{-01}	1.773×10^{-01}	2.34
5.11	357	8.02	1.22×10^{-02}		0.845	4.242×10^{-01}	1.842×10^{-01}	2.30
5.12	381	7.91	1.23×10^{-02}		0.850	4.263×10^{-01}	1.947×10^{-01}	2.19
6.1	0	5.31	1.15×10^{-02}	708 ± 18	0.070	N.D.	N.D.	
6.2	43	7.81	1.23×10^{-02}		0.975	1.683×10^{-01}	1.068×10^{-01}	1.58
6.3	69	7.95	1.22×10^{-02}		1.060	2.393×10^{-01}	1.278×10^{-01}	1.87
6.4	93	8.00	1.24×10^{-02}		1.195	3.241×10^{-01}	2.038×10^{-01}	1.59
6.5	165	8.09	1.26×10^{-02}		1.305	3.396×10^{-01}	1.766×10^{-01}	1.92
6.6	189	8.29	1.28×10^{-02}		1.430	3.397×10^{-01}	1.674×10^{-01}	2.03
6.7	213	8.18	1.29×10^{-02}		1.410	3.509×10^{-01}	1.717×10^{-01}	2.04
6.8	237	8.16	1.30×10^{-02}		1.370	3.580×10^{-01}	1.562×10^{-01}	2.29
6.9	261	8.18	1.30×10^{-02}		1.425	3.792×10^{-01}	1.765×10^{-01}	2.15
6.10	333	8.25	1.30×10^{-02}		1.480	3.958×10^{-01}	2.384×10^{-01}	1.66
6.11	357	8.19	1.30×10^{-02}		1.410	4.024×10^{-01}	1.852×10^{-01}	2.17
6.12	381	8.20	1.30×10^{-02}		1.520	4.031×10^{-01}	1.983×10^{-01}	2.03
7.1	0	5.40	9.99×10^{-02}	0	0.060	N.D.	N.D.	
7.2	43	7.45	1.01×10^{-01}		0.475	2.111×10^{-01}	9.831×10^{-02}	2.15
7.3	69	7.86	1.01×10^{-01}		0.620	3.023×10^{-01}	1.416×10^{-01}	2.13
7.4	93	7.71	1.01×10^{-01}		0.670	3.740×10^{-01}	1.719×10^{-01}	2.18
7.5	165	7.82	1.03×10^{-01}		0.840	4.242×10^{-01}	1.706×10^{-01}	2.49
7.6	189	7.81	1.04×10^{-01}		0.845	4.205×10^{-01}	1.730×10^{-01}	2.43
7.7	213	7.84	1.05×10^{-01}		0.905	4.262×10^{-01}	1.746×10^{-01}	2.44
7.8	237	7.85	1.07×10^{-01}		0.890	4.612×10^{-01}	2.050×10^{-01}	2.25
7.9	261	7.85	1.08×10^{-01}		0.935	4.641×10^{-01}	2.176×10^{-01}	2.13
7.10	333	7.82	1.07×10^{-01}		0.980	4.970×10^{-01}	2.439×10^{-01}	2.04
7.11	357	7.86	1.07×10^{-01}		0.970	5.127×10^{-01}	2.424×10^{-01}	2.11
7.12	381	7.86	1.09×10^{-01}		1.005	5.291×10^{-01}	2.574×10^{-01}	2.06

8.1	0	5.37	1.01×10^{-01}	735 ± 11	0.070	N.D.	N.D.	
8.2	43	7.71	9.90×10^{-02}		0.960	1.551×10^{-01}	1.086×10^{-01}	1.43
8.3	69	7.77	9.84×10^{-02}		1.060	1.888×10^{-01}	8.814E-02	2.14
8.4	93	7.77	1.00×10^{-01}		1.045	2.323×10^{-01}	1.459×10^{-01}	1.59
8.5	165	7.89	1.00×10^{-01}		1.185	2.791×10^{-01}	1.670×10^{-01}	1.67
8.6	189	7.93	1.02×10^{-01}		1.270	2.946×10^{-01}	1.649×10^{-01}	1.79
8.7	213	8.00	1.03×10^{-01}		1.300	3.107×10^{-01}	1.985×10^{-01}	1.57
8.8	237	7.97	1.04×10^{-01}		1.325	3.388×10^{-01}	2.059×10^{-01}	1.65
8.9	261	8.02	1.05×10^{-01}		1.365	3.546×10^{-01}	2.123×10^{-01}	1.67
8.10	333	8.00	1.05×10^{-01}		1.420	3.881×10^{-01}	2.019×10^{-01}	1.92
8.11	357	8.11	1.05×10^{-01}		1.515	4.004×10^{-01}	2.469×10^{-01}	1.62
8.12	381	8.09	1.04×10^{-01}		1.570	4.056×10^{-01}	2.441×10^{-01}	1.66

***** A zero value of biomass corresponds to inorganic control experiments only in the presence of olivine. N.D. refers to a value “not determined”

Table 2. Calculated olivine dissolution rates

Exp #	Time (hours)	Reactor vol (L)	$R_{(OL)}$* (mol cm^{-2} s^{-1})	log $R_{(OL)}$
1.1	0	1		
1.2	43	0.97		
1.3	69	0.94	3.16×10^{-13}	-12.5
1.4	93	0.91	1.30×10^{-13}	-12.9
1.5	165	0.88	8.54×10^{-14}	-13.1
1.6	189	0.85	8.29×10^{-14}	-13.1
1.7	213	0.82	7.67×10^{-14}	-13.1
1.8	237	0.79	6.16×10^{-14}	-13.2
1.9	261	0.76	2.27×10^{-13}	-12.6
1.10	333	0.73	6.65×10^{-14}	-13.2
1.11	357	0.7	4.17×10^{-14}	-13.4
1.12	381	0.67	1.51×10^{-14}	-13.8
2.1	0	1		
2.2	43	0.97		
2.3	69	0.94	9.61×10^{-14}	-13.0
2.4	93	0.91	3.48×10^{-13}	-12.5
2.5	165	0.88	1.08×10^{-13}	-13.0
2.6	189	0.85	1.32×10^{-13}	-12.9
2.7	213	0.82	6.03×10^{-14}	-13.2
2.8	237	0.79	1.79×10^{-13}	-12.7
2.9	261	0.76	1.78×10^{-13}	-12.8
2.10	333	0.73	5.44×10^{-14}	-13.3
2.11	357	0.7	9.92×10^{-14}	-13.0
2.12	381	0.67	5.38×10^{-14}	-13.3
3.1	0	1		
3.2	43	0.97		
3.3	69	0.94	1.66×10^{-13}	-12.8

3.4	93	0.91	2.99×10^{-13}	-12.5
3.5	165	0.88	1.04×10^{-13}	-13.0
3.6	189	0.85	1.06×10^{-13}	-13.0
3.7	213	0.82	8.96×10^{-14}	-13.0
3.8	237	0.79	1.18×10^{-13}	-12.9
3.9	261	0.76	2.56×10^{-13}	-12.6
3.10	333	0.73	5.96×10^{-14}	-13.2
3.11	357	0.70	6.42×10^{-14}	-13.2
3.12	381	0.67	7.80×10^{-14}	-13.1
4.1	0	1		
4.2	43	0.97		
4.3	69	0.94	2.71×10^{-13}	-12.6
4.4	93	0.91	8.78×10^{-13}	-12.1
4.5	165	0.88		
4.6	189	0.85	5.69×10^{-14}	-13.2
4.7	213	0.82	1.28×10^{-13}	-12.9
4.8	237	0.79		
4.9	261	0.76	4.39×10^{-13}	-12.4
4.10	333	0.73	3.59×10^{-14}	-13.4
4.11	357	0.70		
4.12	381	0.67	3.96×10^{-14}	-13.4
5.1	0	1		
5.2	43	0.97		
5.3	69	0.94	3.55×10^{-13}	-12.4
5.4	93	0.91	3.95×10^{-13}	-12.4
5.5	165	0.88	1.48×10^{-13}	-12.8
5.6	189	0.85	1.79×10^{-13}	-12.7
5.7	213	0.82	1.25×10^{-13}	-12.9
5.8	237	0.79	1.56×10^{-13}	-12.8
5.9	261	0.76	1.63×10^{-13}	-12.8

5.10	333	0.73	9.68×10^{-14}	-13.0
5.11	357	0.70	8.50×10^{-14}	-13.1
5.12	381	0.67	2.03×10^{-14}	-13.7
6.1	0	1		
6.2	43	0.97		
6.3	69	0.94	6.12×10^{-13}	-12.2
6.4	93	0.91	7.92×10^{-13}	-12.1
6.5	165	0.88	4.83×10^{-14}	-13.3
6.6	189	0.85	3.84×10^{-16}	-15.4
6.7	213	0.82	1.05×10^{-13}	-13.0
6.8	237	0.79	6.65×10^{-14}	-13.2
6.9	261	0.76	1.98×10^{-13}	-12.7
6.10	333	0.73	5.16×10^{-14}	-13.3
6.11	357	0.70	6.19×10^{-14}	-13.2
6.12	381	0.67	6.15×10^{-15}	-14.2
7.1	0	1		
7.2	43	0.97		
7.3	69	0.94	7.86×10^{-13}	-12.1
7.4	93	0.91	6.70×10^{-13}	-12.2
7.5	165	0.88	1.56×10^{-13}	-12.8
7.6	189	0.85		
7.7	213	0.82	5.38×10^{-14}	-13.3
7.8	237	0.79	3.27×10^{-13}	-12.5
7.9	261	0.76	2.69×10^{-14}	-13.6
7.10	333	0.73	1.02×10^{-13}	-13.0
7.11	357	0.70	1.46×10^{-13}	-12.8
7.12	381	0.67	1.54×10^{-13}	-12.8
8.1	0	1		
8.2	43	0.97		

8.3	69	0.94	2.91×10^{-13}	-12.5
8.4	93	0.91	4.06×10^{-13}	-12.4
8.5	165	0.88	1.46×10^{-13}	-12.8
8.6	189	0.85	1.45×10^{-13}	-12.8
8.7	213	0.82	1.51×10^{-13}	-12.8
8.8	237	0.79	2.63×10^{-13}	-12.6
8.9	261	0.76	1.48×10^{-13}	-12.8
8.10	333	0.73	1.04×10^{-13}	-13.0
8.11	357	0.70	1.15×10^{-13}	-12.9
8.12	381	0.67	4.88×10^{-14}	-13.3

***** Olivine dissolution rates after the calculation procedure $R = (d[Mg^{2+}]/dt)/SA$

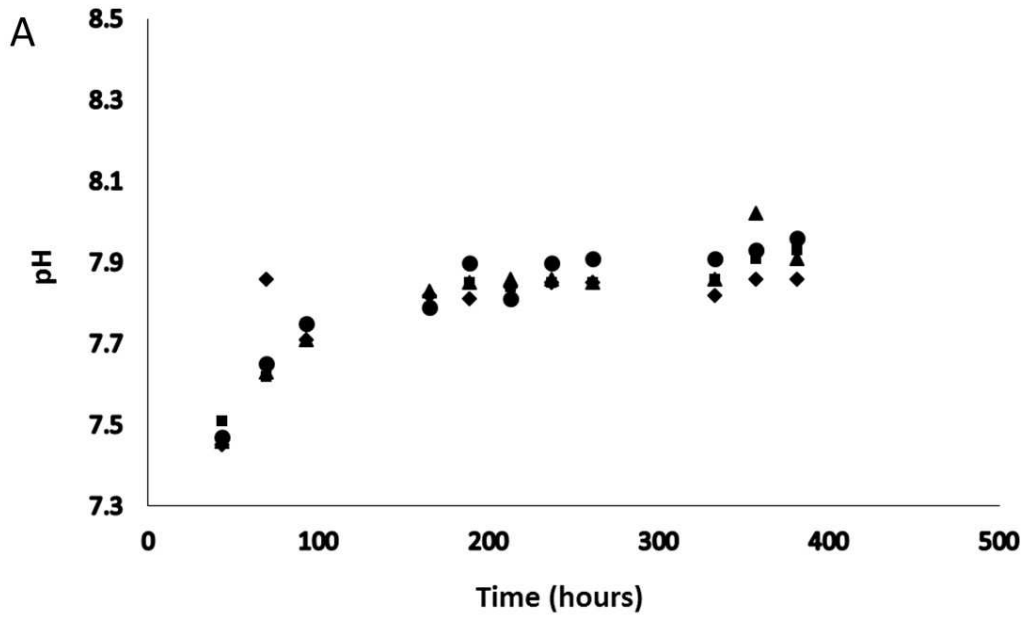

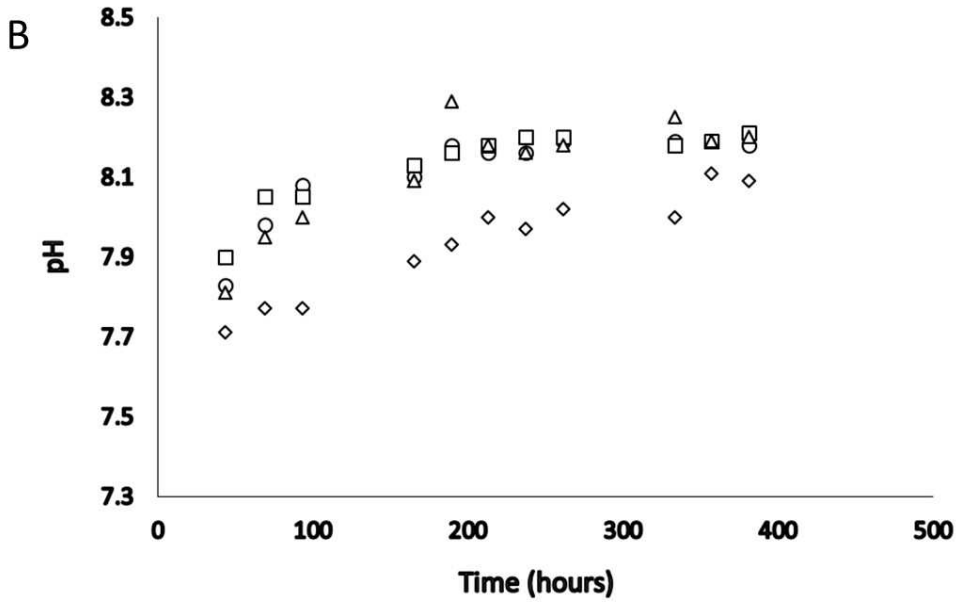

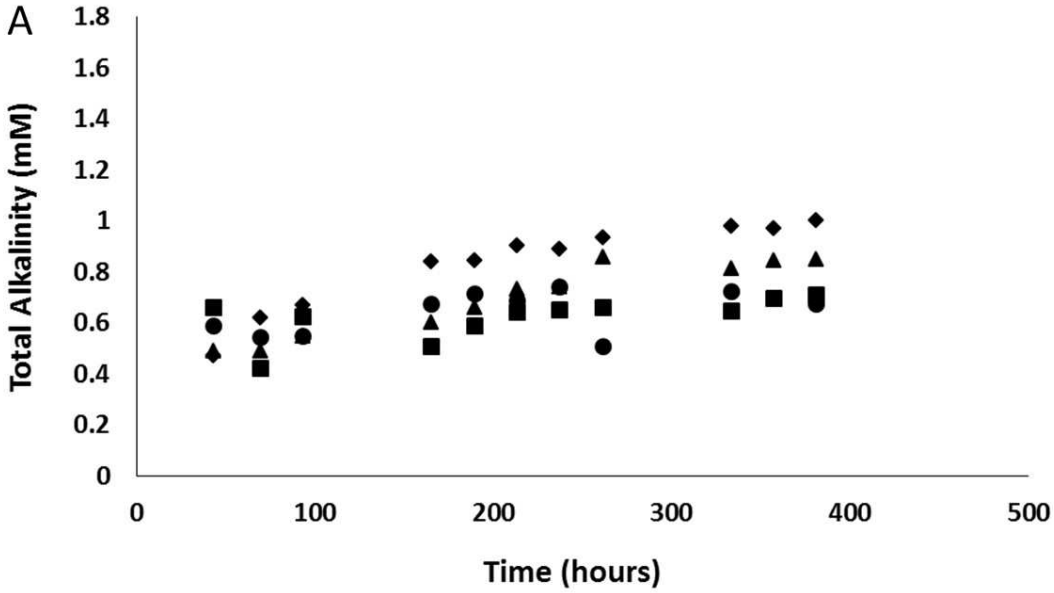

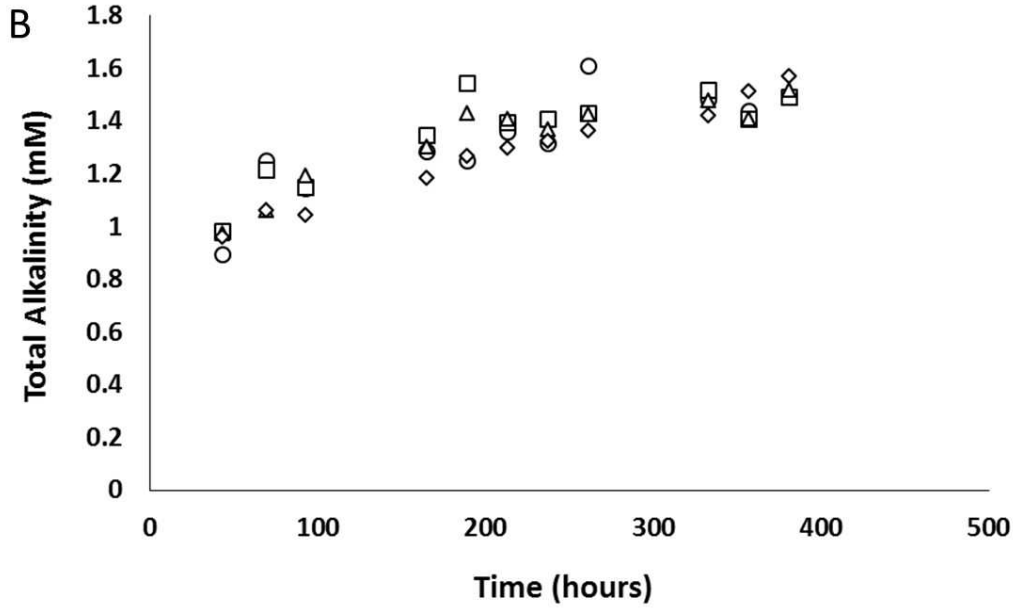

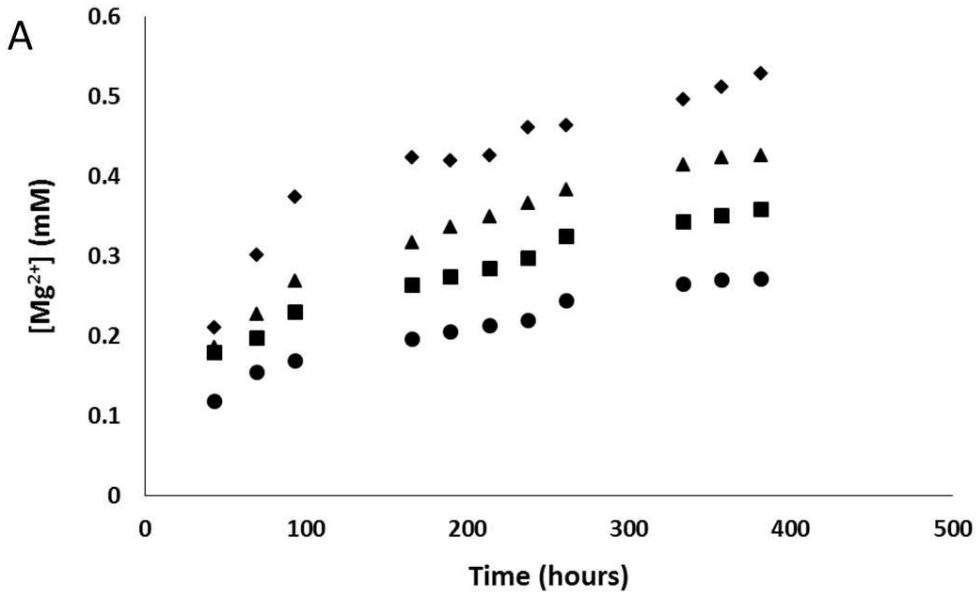

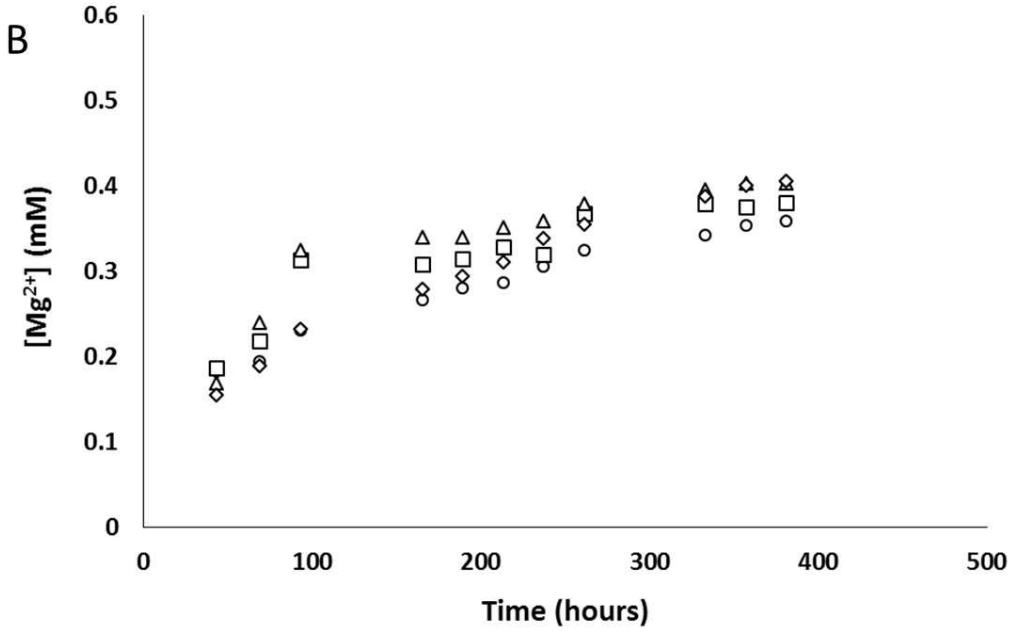

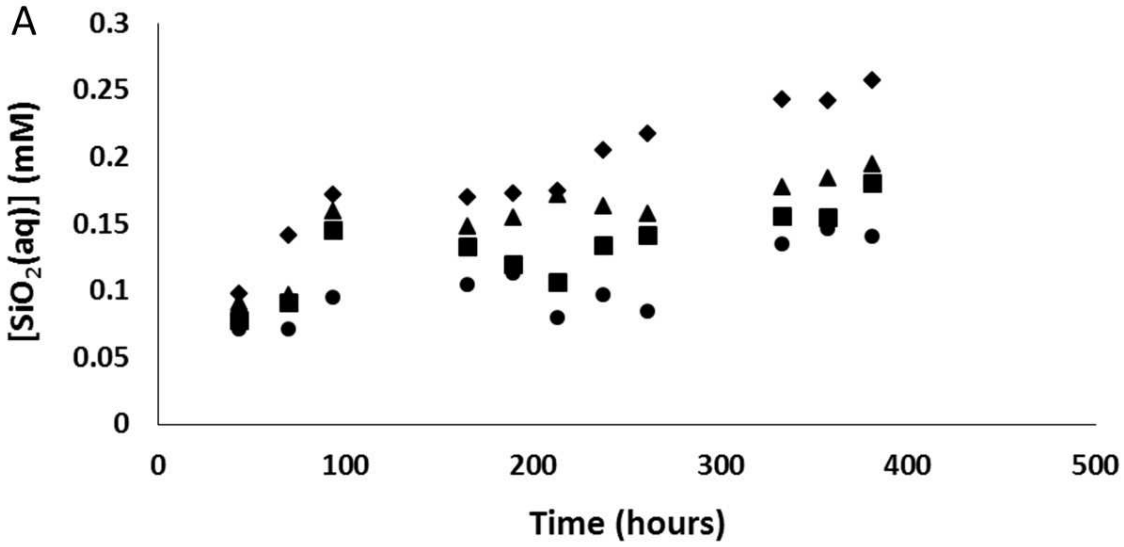

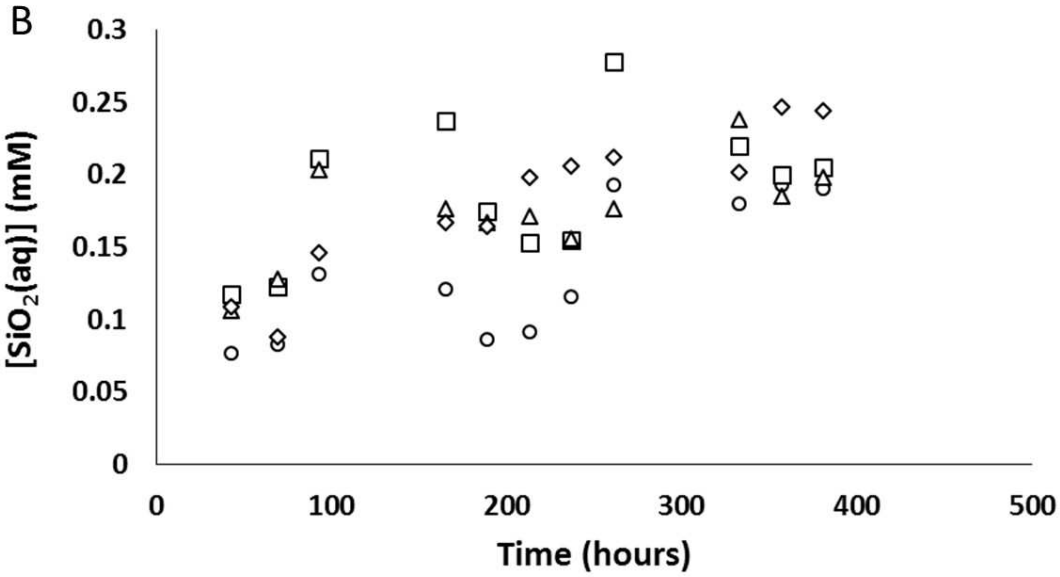

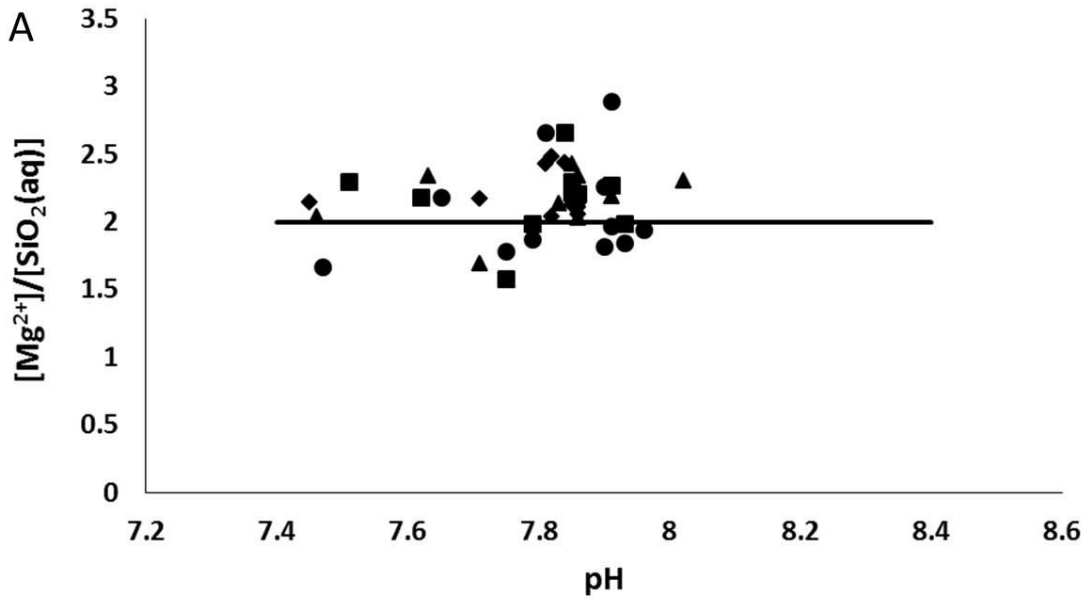

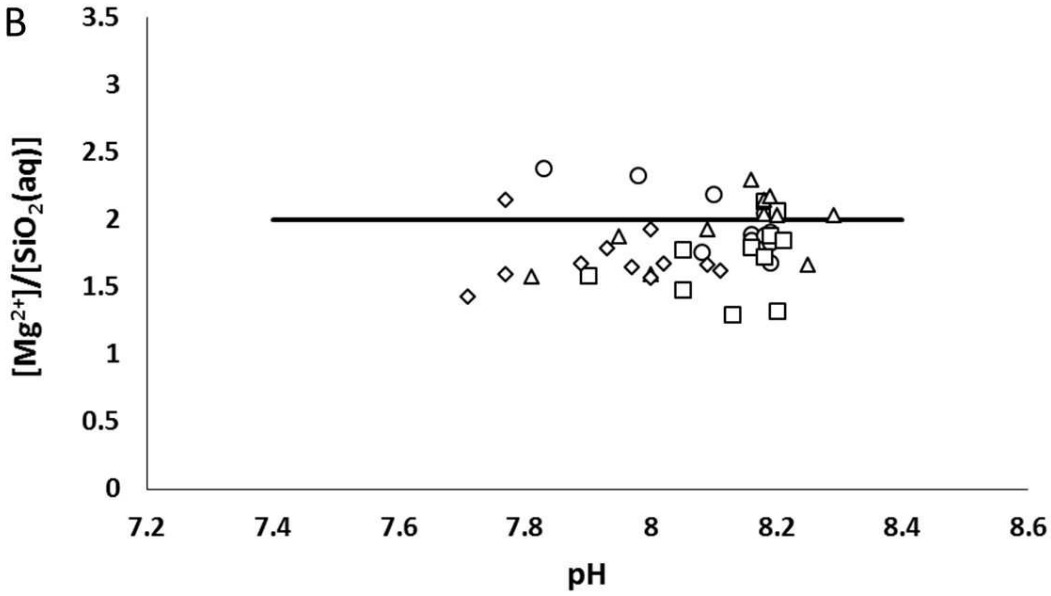

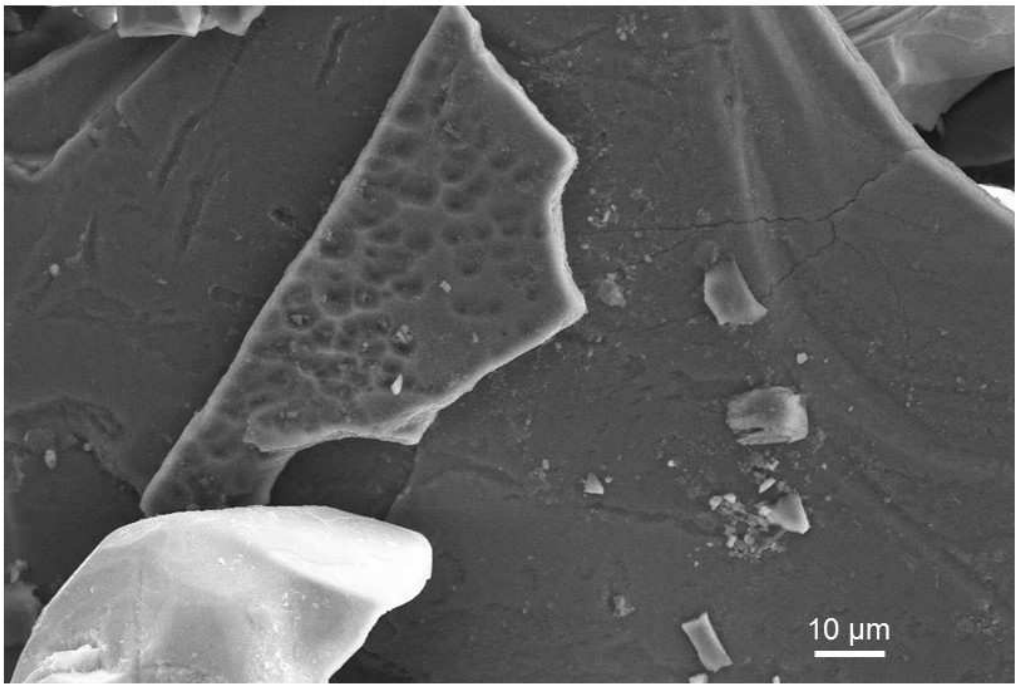

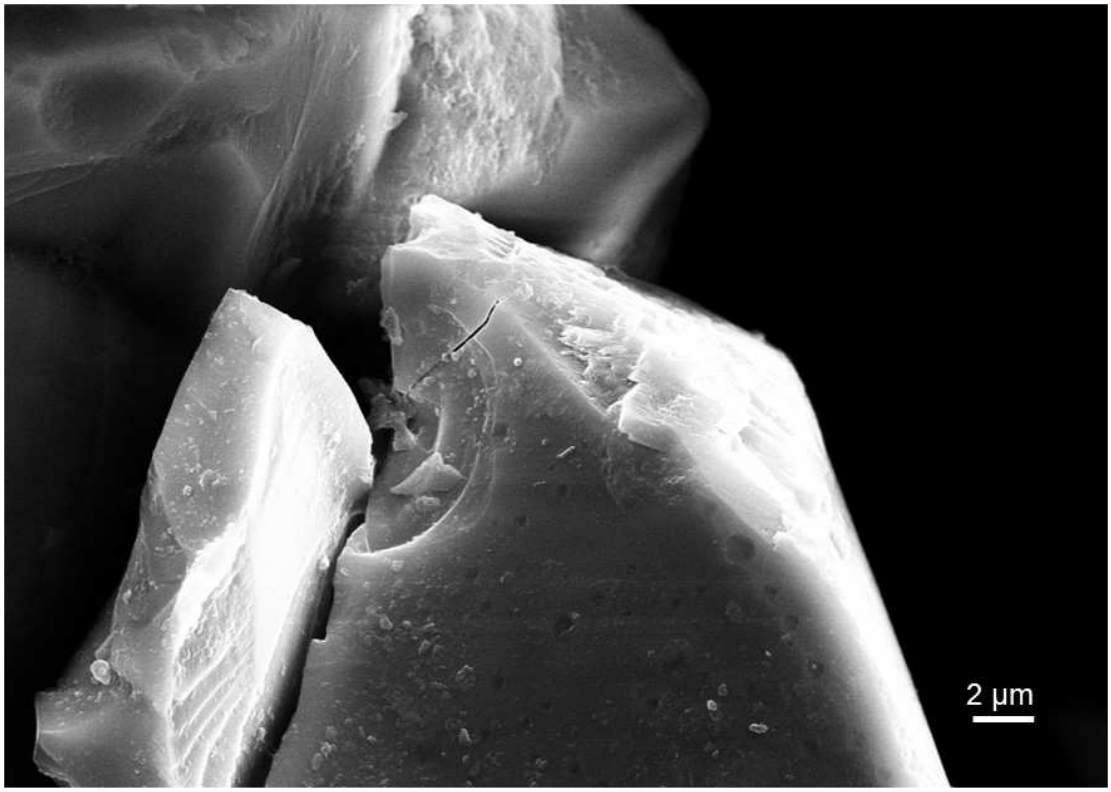

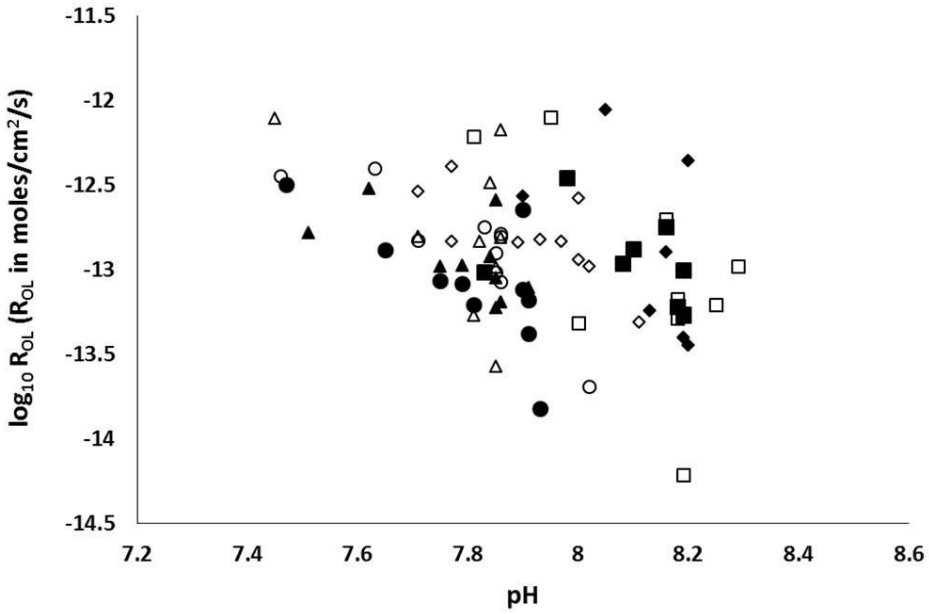

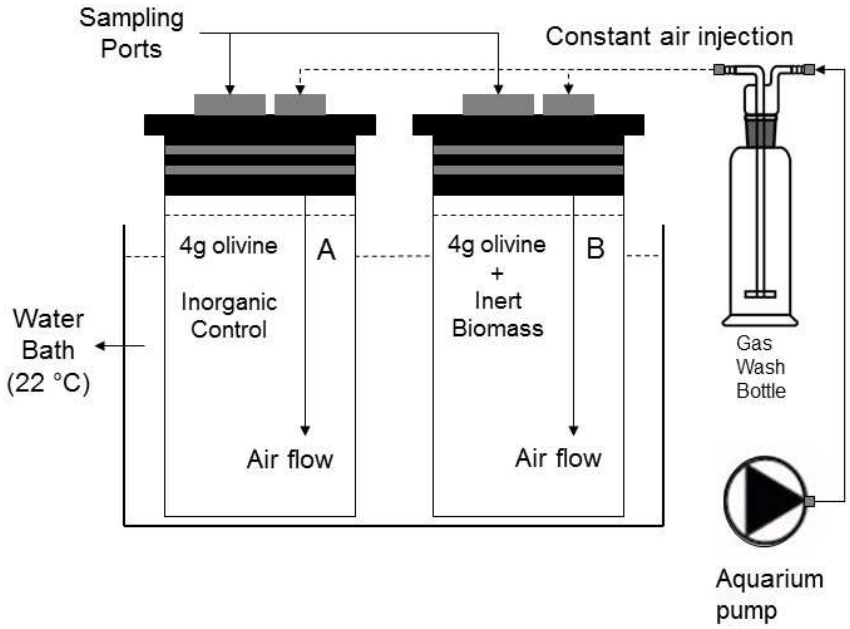

Effects of inert *Synechococcus* sp. cyanobacteria biomass on olivine dissolution: implications for the application of enhanced weathering methods

Sebastian Weber and Raul E. Martinez*

Institut für Geo- und Umweltnaturwissenschaften, Mineralogie-Petrologie, Albert-Ludwigs-Universität Freiburg, D-79104 Freiburg, Germany.

Manuscript Highlights:

(1) Interaction of inert cyanobacteria biomass with olivine inhibits mineral dissolution.

(2) Inert biomass cell surface functional groups may interact with >Mg-O active sites.

(3) No enhancement observed in the rates of olivine dissolution in presence of inert biomass.

*corresponding author